Hydrogen mediated transport of Sn to Ru film surface

Nadir Faradzhev[a)]
Physics Department, Rutgers University, 136 Frelinghuysen Road, Piscataway, New Jersey 08854

Vadim Sidorkin
Faculty of Applied Sciences, TU Delft, Lorentzweg 1, 2628 CJ Delft, The Netherlands

(Received 21 October 2008; accepted 20 January 2009; published 19 February 2009)

The authors report on the interaction of atomic hydrogen with Sn and thin Ru film at room temperature. The study is done using a combination of photoelectron and low energy ion scattering spectroscopies as well as scanning electron microscopy. The adsorption of hydrogen on a Sn surface leads to the formation of stannane (SnH_4), which dissociatively adsorbs on the surface of polycrystalline Ru film. In the range of effective Sn coverages studied (up to 1 ML), the resulting overlayer consists of randomly distributed three-dimensional islands with average size below 40 nm occupying up to several percent of the surface area. Nucleation of Sn is observed presumably at defect sites (e.g., grain boundaries). Ion scattering data are found consistent with Volmer–Weber growth mode: no initial transition wetting layer formation is detected. Oxidation of Sn islands on a Ru surface at room temperature results in the formation of SnO. Neither metallic nor oxidation states of Sn higher than Sn^{2+} are observed by photoelectron spectroscopy. © *2009 American Vacuum Society.* [DOI: 10.1116/1.3081968]

I. INTRODUCTION

Bimetallic systems are important for industrial applications oriented on catalysis.[1–3] Ru–Sn catalyst has been recognized as a promising system for selective hydrogenation of a carbonyl group.[4] The selectivity is explained in terms of a strong interaction between the C=O group with the tin oxide. The proximity of Sn to the noble metal and the tin oxidation state are crucial to produce an active and selective catalyst. The distribution of the ionic tin in the catalyst is affected by the preparation procedure, e.g., sol-gel process,[5] coimpregnation of two different ruthenium and tin precursors,[6] or production from a single source precursor containing both metals.[7]

A large number of fundamental studies of bimetallic surfaces are focused on the influence of structural parameters on the chemical reactivity of the system.[2,8] Depending on the surface temperature, the interaction of a promoter (e.g., Sn) with a single crystal surface of a noble metal catalyzing a reaction may lead to formation of an ordered surface alloy or a thin film with abrupt interface. It has been observed that atomically rough, high energy surfaces may be morphologically unstable during reaction conditions.[9] In contrast to the closed packed faces, the high-index surfaces may undergo massive structural rearrangements (e.g., faceting) when covered by a metallic film. It is also shown that film growth mode on nanofaceted surface may be very different from a growth mode on the flat substrate.[10] Surfaces with polycrystalline morphology and grain boundaries may also exhibit a growth mode different from a surface of a single crystal.

Formation of surface alloys is driven by difference in surface free energies. Surface alloying of Sn deposited on Pt(111) and Pd(111) occurs at 300–400K.[11] The exothermic heats of formation of specific intermetallic compounds serve as a sufficient thermodynamic driving force for the formation of Sn–Pt alloy. A random alloy of increasing thickness was also detected at 300 K for vapor deposited Sn on Rh(111).[12] The phase diagram of Sn–Ru system is thoroughly studied.[13,14] The solubility ranges of Sn in Ru and Ru in Sn are very small.[15] On the basal plane of ruthenium, Sn prefers to segregate due to its much lower surface free energy.[16] The intermixing and surface alloy bonding with Sn adatoms require a large thermal excursion to occur.[14] Sn deposition on Ru(0001) at temperatures >600 K and upon annealing to 1000 K leads to alloy formation with surface Sn:Ru atom ratio of 2:1.[17] However, vapor deposition of Sn on this surface at low temperature (330 K) does not produce surface alloy, but rather results in a Stranski–Krastanov growth mode, i.e., formation of the first uniform monolayer followed by a three-dimensional (3D) growth.[17]

It is reported that high pressure oxidation of ultrathin Sn films on Pd(111) at 300 K results exclusively in SnO formation in the absence of intermediate or higher oxides.[18] Surface Pd oxide has not been formed presumably because of strong preexisting Sn to Pd charge transfer and the low dimensionality of the oxidized Sn overlayer. Recent studies have suggested that Zn(II) can be reduced by chemisorbed hydrogen to form $Ru-Zn^{2+}/Ru-Zn$ distribution on the catalyst surface.[19] This is confirmed by theoretical study focused on effect of Zn^{2+}/Zn layer on dissociation of H_2 on Ru(0001).[20] They found that Zn^{2+} has a dramatic influence on the electron delocalization between molecular orbit on H_2 and valence orbits of atop Ru atom increasing H_2 dissociation barrier and resulting in zones of sparse chemisorbed H around Zn^{2+}. It is shown that flowing of atomic H to oxidized thin Ru film can reduce Ru^{n+} to metal.[21] In a solid-gas reaction between metal and H, ruthenium forms no stable binary

[a)]Author to whom correspondence should be addressed; also at National Institute of Standards and Technology, Gaithersburg, MD 20899; electronic mail: nadir.faradzhev@nist.gov

hydride,[22] but Sn does produce a stable covalent compound SnH_4, which is a very volatile hydride (boiling point 221 K) decomposing at room temperature (RT).[23,24] Stannanes are widely used in electronic devices in the initial step of chemical vapor deposition processes.[25,26]

In addition to catalytic interest, Sn contamination of Ru-coated optics for extreme ultraviolet (EUV) lithography may become a potential problem[27,28] since the introduction of new powerful Sn-based laser-produced plasma sources. Hydrogen being considered for EUV optics cleaning[21] may react with Sn to yield a volatile hydride, which, in turn, may subsequently dissociate on chemically active surfaces spreading contamination all over a lithography tool.

In this article, we focus on hydrogen promoted transport of Sn to the surface of thin polycrystalline Ru film. We discuss the structure of Sn layer, the influence of high pressure oxidation on the morphology, and Sn oxidation states on the Ru surface.

II. EXPERIMENT

The experiments were performed under ultrahigh vacuum conditions at RT using three techniques: x-ray photoelectron spectroscopy (XPS), low energy ion scattering (LEIS) spectroscopy, and scanning electron microscopy (SEM).

The morphology of Sn layer grown on the surface of Ru was imaged by a field-emission scanning electron microscope (FEI Strata DB235) operated in secondary electron mode. The distance between sample and objective lens was about 5 mm during the imaging. The accelerating voltage was 5 kV.

The XPS system was a commercial Axis Ultra spectrometer (Kratos Analytical) with a base pressure of 1×10^{-9} Torr. The source was monochromatized Al $K\alpha$ radiation (1486.6 eV) operated at 90 W; the take off angle was 45°. Spot of analysis was an ellipse with the area ~0.8 mm². Analyzer and transfer lenses operated at fixed analyzer transmission mode. Survey spectra were an average of three scans with 1 eV/step and were acquired at a pass energy of 80 eV. High-resolution spectra were acquired by averaging five scans at 0.2 eV/step with a pass energy of 20 eV.

The ion gun of the sputtering system was adapted for LEIS spectroscopy. In our measurements, a 1 keV He^4 ion beam (10 nA beam current; 1 mm² beam size) was incident at the surface at 45° with respect to the surface plane. The ions scattered at 135° were detected by analyzer operating in positive charged particle detection mode. Spectra were taken in the full energy range up to 1 keV with a 0.5 eV/step and a dwell time of 300 ms. Both XPS and LEIS spectra were fitted using CASAXPS software.[29]

The sample was a polycrystalline Ru film (31 nm thick) grown on the rectangular cut of the silicon wafer ($18 \times 12 \times 0.6$ mm³). The sample was mounted on aluminum puck attached to the XPS sample holder. The assembly efficiently dissipates heat load.

Hydrogen exposures were performed in the preparation chamber with the base pressure $\sim 1 \times 10^{-8}$ Torr. Molecular hydrogen (H_2; Matheson Tri Gas, 99.9999%) was exposed through a leak valve and cracked[30] directly on the high temperature iridium filament (∅ 0.008 in. iridium wire; 99.9%, e-Filaments, LLC) shaped as Fermat's (parabolic) spiral. The filament was placed approximately 4 cm in front of the sample surface and operated at 2000 °C. The partial pressure of the H_2 gas was maintained at the level 5×10^{-4} Torr. The filament operated in a sequence of heating/cooling cycles to keep surface temperature below 330K and to avoid substantial radiative heat load and the heat associated with hydrogen recombination. The ·H doses (cm^{-2}) shown in this article are based on an average flux of 1.8×10^{16} s^{-1} cm^{-2} producing by the source at the sample surface. This flux is calculated using Hertz–Knudsen formula for the H_2 molecules impinging upon the filament surface, which cracks 50% of the molecules. The mean free path of hydrogen atoms between collisions (leading to the recombination) is assumed 4 cm. Our estimation is in general agreement with the experimentally measured ·H flux produced by thermal source.[30–32]

The source of Sn was a lead-free soft soldering wire (Stan Rubinstein Assoc., Inc.) composed of pure Sn. The solder is melted on a 2.5 mm diameter loop made of thin Cu wire (∅ 0.2 mm). This design produced an effective Sn surface area 4 mm² faced toward the sample. The source of Sn was cleaned in ultrasonic washer with acetone followed by cleaning in ethanol and in ultrapure water, then dried with nitrogen flow, and, finally, mounted close to the edge of the sample at tilt angle 45° and 1 mm above its surface. The analysis spot was at the opposite side of the sample approximately 12 mm away from the loop with Sn. During experiments, the source was kept at RT.

III. RESULTS

A. Exposure of Ru film to ·H in the presence of Sn

Photoelectron spectra recorded for Ru film exposed to various doses of atomic H are illustrated by Fig. 1. Tag "Sn+H" in the graph indicates that exposures are done in the presence of Sn. The spectra show evolution of Sn $3d$/Ru $3p$ energy region. The dash lines represent the results of fitting. Initial spectrum taken before admission of H_2 is marked "as installed." It reveals two core level emissions lines Ru $3p_{3/2}$ (461.3 eV) and Ru $3p_{1/2}$ (483.6 eV) associated with Ru film.

Subsequent H exposure results in dramatic change in this region: H dose 1.6×10^{19} cm^{-2} leads to the increase in the total Ru $3p$ signal as a result of the removal of an overlayer of air gases (carbon monoxide, dissociated fragments of hydrocarbons, and water) and as a result of reduction in surface oxides by chemically active hydrogen atoms.[21,33] Figure 2(a) illustrates a rapid drop of O $1s$ peak integral after the same H dose. It is accompanied by a sudden increase in Ru $3d$ signal. The corresponding spectra are shown in Fig. 3 (O $1s$ region) and Fig. 4 (Ru $3d$ region). First H exposure also leads to formation of a new feature in Ru $3p$ region at around 471 eV (Fig. 1). We attribute this weak bump to inelastic scattering of the photoelectrons.[34]

The spectrum measured after H dose 1.6×10^{19} cm^{-2} (Fig. 1) exhibits a new, weak feature at ~493 eV. The sub-

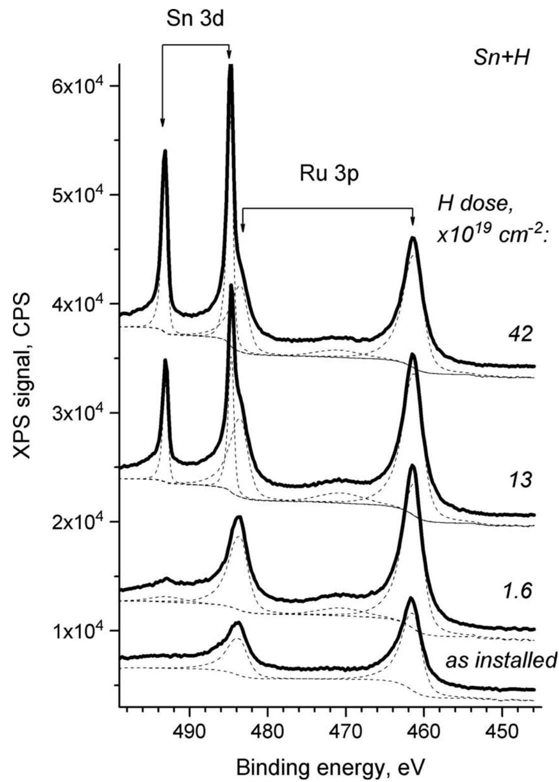

FIG. 1. Photoelectron spectra (mono-Al $K\alpha$) measured in Sn $3d$/Ru $3p$ energy region during sample exposure to the atomic hydrogen in the presence of Sn. The dash lines represent fittings which are shifted vertically for clarity.

sequent H exposure reveals a strong pair of Sn lines: Sn $3d_{5/2}$ (484.5 eV) and Sn $3d_{3/2}$ (492.9 eV). Photoelectron emission from Sn goes up with H dose indicating the growth of Sn overlayer on Ru surface. The dynamics is illustrated by plot in Fig. 2(a). Effective thickness of Sn layer deposited after ·H dose 4.2×10^{20} cm^{-2} is $\approx$2.5 Å as estimated from ratio of Sn $3d$ to Ru $3d$ signals. Corresponding effective coverage is $\approx$0.85 ML (based on an average interatomic distance of 2.99 Å in bulk Sn with a density of 7.365 g/cm^3).

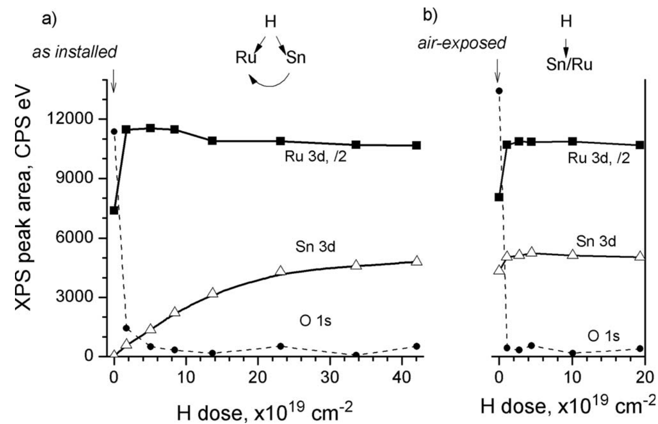

FIG. 2. Variation in the XPS peak areas in O $1s$ (circles), Sn $3d$ (triangles), and Ru $3d$ (squares) energy regions during sample exposure to atomic H in the presence of Sn (a) and the exposure after surface oxidation and removal of Sn source (b).

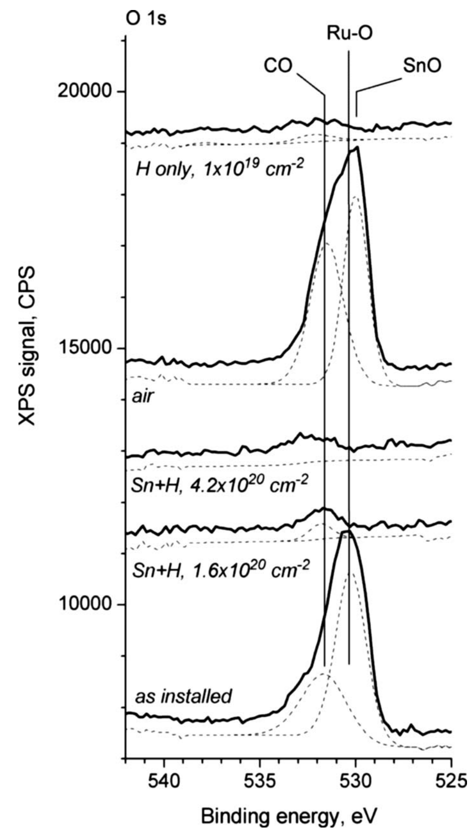

FIG. 3. Photoelectron spectra measured in O $1s$ region at various stages of sample processing: before (as installed) and after sample exposure to the atomic H in the presence of solder (Sn+H) followed by air exposure (air) and subsequent H exposure with Sn source removed (H only). The plot illustrates oxidation, reduction, and reoxidation of the surface.

B. Distribution of Sn across the surface

We measured the distribution of Sn concentration across Ru surface after ·H dose 1.3×10^{20} cm^{-2}. The variation in

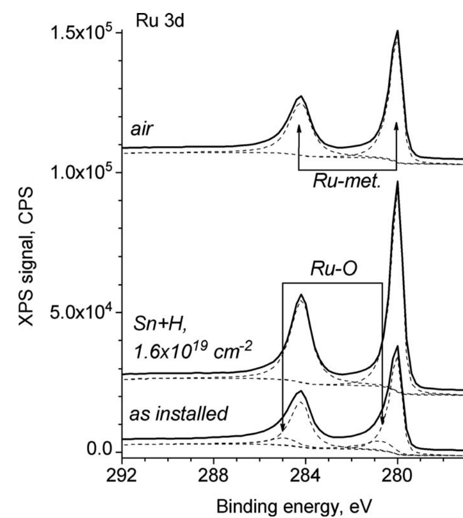

FIG. 4. Photoelectron spectra measured in Ru $3d$/C $1s$ energy region for the bare Ru film before H exposure (as installed) and then after 1.6 $\times10^{19}$ cm^{-2}·H in the presence of solder (Sn+H). The curve *air* is for oxidized Sn/Ru surface (after dose 4.2×10^{20} cm^{-2}·H in the presence of Sn followed by air exposure).

Sn 3d XPS signal was very subtle as we moved away from the Sn source: the difference of the signals between two spots located 15 mm apart was ~10% only. Assuming radial distribution of Sn emission from a point source, one can expect the surface concentration of Sn to be inversely proportional to R^2, where R is the distance from the Sn source. For our experimental geometry, this would mean a 50 times drop of the Sn signal across the surface. In contrast, we observe a very weak dependence of Sn concentration on R. This indicates that a precursor carrying out Sn to Ru surface originates from a diffuse source. Therefore, thermal evaporation of Sn is not responsible for the Sn transport. Besides, the vapor pressure of Sn is very low: $\ll 10^{-13}$ Torr (Ref. 35) at RT. We rule out excessive heating of Sn (due to the radical recombination or radiative heating) as our design of the sample/holder/source assembly dissipates heat efficiently. In the text below, we will ascribe Sn transport to the formation of tin hydride followed by its dissociation on the catalytically active Ru surface.

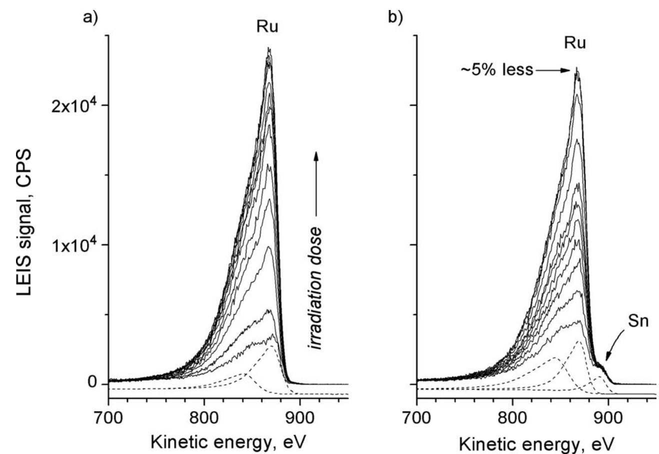

FIG. 5. LEIS spectra (He^4, 1 keV) measured for bare Ru (a) exposed to 1.6×10^{19} cm^{-2}·H before Sn source was introduced into the chamber and (b) after 4.2×10^{20} cm^{-2}·H in the presence of Sn (b). The different curves correspond to various doses of He ions. The dash lines represent fits. For the same He^+ doses, the signal from Ru is about 5% less from the surface containing Sn as compared to the clean surface.

C. Effect of ·H on the Sn source

The effect of atomic H on Sn source was studied additionally. The XPS spectra measured from Sn source surface were taken before the first hydrogen exposure and after two cumulative doses of hydrogen: 1.6×10^{19} and 4.2×10^{20} cm^{-2} (not shown). Initially, the surface of the source contained mainly SnO_2 covered or intermixed with carbonaceous species. The ·H dose 1.6×10^{19} cm^{-2} led to the reduction in Sn and a complete removal of carbon. Sn 3$d_{5/2}$ peak revealed 2.4 eV chemical shift from 487.3 to 484.9 eV indicating the transition from Sn(IV) to metallic Sn.[36] Some residue (sub-at. %) of Sn(II) was, however, seen through all H exposures as evidenced by a small Sn 3$d_{5/2}$ peak at 486.8 eV.

D. Surface occupation

The surface occupation of Ru film was characterized with LEIS.[37] Figure 5 shows sequential spectra detected with increasing He^+ dose (a) for bare Ru film exposed to 1.6×10^{19} cm^{-2} ·H with no Sn in the chamber and (b) for Ru film exposed to 4.2×10^{20} cm^{-2}·H in the presence of Sn.

The spectra in Fig. 5(a) reveal an increase in the total signal with ion irradiation time. This growth slows down at higher He^+ doses and saturates after ~40 min of ion gun operation. Fitting of the spectra (dash lines; asymmetric Gaussian–Lorentzian line shape) requires inclusion of two components at ~840 and at ~875 eV. We attribute both features to scattering of He by Ru atoms. The lower energy feature at ~840 eV may result from backscattering of He in deeper layers accompanied by reionization process.[37] XPS did not detect any element on the surface (except Ru) that may contribute to the signal at these kinetic energies. Very similar low energy tail in the spectrum of 1 keV He^+ scattered from bare Ru is also present in two earlier studies: of Al growth on Ru(0001) (Ref. 38) and of erosion of Ru-coated glancing incidence mirrors.[39]

Spectra recorded after ·H dose 4.2×10^{20} cm^{-2} in the presence of Sn [Fig. 5(b)] show the same tendency: the raise of the Ru signal with He dose followed by saturation. In both cases (with and without Sn), we assign the increase in Ru signal to the He-promoted recombination and desorption of hydrogen from Ru surface. The area under Ru components of the saturated spectrum in Fig. 5(b) is ~5% less than that in Fig. 5(a), indicating that the effective surface area of Ru is also 5% less as compared to the Sn-free surface.

The spectra in the Fig. 5(b) reveal an additional peak at ~895 eV. The kinetic energy is consistent with scattering of He by Sn atoms. In contrast to Ru, the area of Sn peak does not change with the He^+ exposure time; it remains virtually unaltered, indicating no change in the total area occupied by Sn on the surface.

We also studied the effect of prolonged He^+ bombardment on the surface composition. XPS signal in Sn 3d region measured after taking LEIS sequence shown in Fig. 5(b) dropped down to ~70% of its initial value (i.e., before LEIS), indicating the decrease in the total concentration of Sn due to ion-induced processes (e.g., desorption or bulk diffusion).

E. Surface morphology

SEM was employed to examine the surface of the sample after ·H dose 4.2×10^{20} cm^{-2} in the presence of Sn. The sample was taken out of analysis chamber and transported to the SEM facility. The SEM image of small area 1.5×1.5 μm^2 of air-exposed Ru film with Sn overlayer is shown in Fig. 6. It reveals a uniform morphology with rarely distributed particles of unequal sizes up to ~40 nm in diameter. The particles appear as bright objects with stronger secondary electron emission signal as compared to the other surface areas. These particles (or islands) are homogenous, mostly rounded and formed presumably by Sn. The SEM images of unexposed sample (not shown here) do not reveal these objects. A slightly higher secondary electron yield

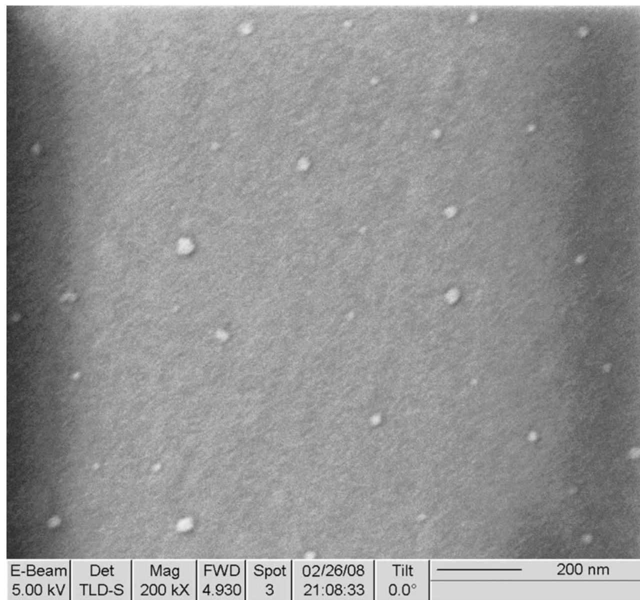

FIG. 6. SEM image (5 keV) measured for Ru-coated sample exposed to atomic hydrogen in the presence of tin. The image area is 1.5×1.5 μm^2. Corresponding effective Sn coverage determined by XPS is ≈ 1 ML. The image reveals islands with range of diameters up to ~40 nm occupying several percent of the surface area. The cluster heights deduced from XPS and SEM data are up to 20 nm. Tin probably nucleates at the crossroads of grain boundaries.

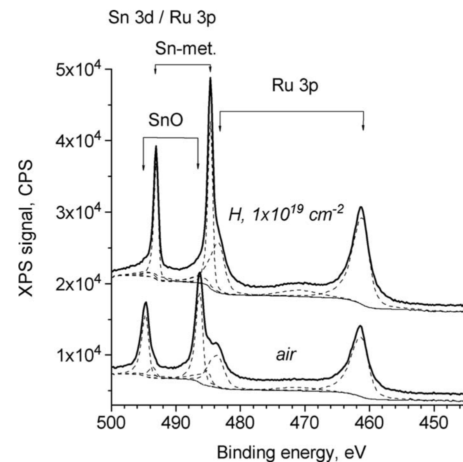

FIG. 7. Photoelectron spectra measured in Sn $3d$/Ru $3p$ region for Ru film covered by Sn (~1 ML). The sample was oxidized by exposing it to the air in preparation chamber to mimic high pressure oxidation (curve *air*). The oxidation was followed by 1×10^{19} $cm^{-2} \cdot H$ with no Sn source (H, 1×10^{19} cm^{-2}).

(SEY) from Sn is expected. Indeed, maximum SEY δ_m from Ru is ~1.1,[40] and from Sn it is 1.35.[35,40] The yield from SnO_2 is 3.2.[35] In Sec. III F, we will show that our air-exposed sample contains Sn^{2+}; Ru remains in the metallic form. Hence, a brighter SEM image from Sn is anticipated.

F. Air exposure

We also studied the effect of high pressure oxidation on the Ru film with Sn overlayer. Figure 3 shows the evolution of O $1s$ energy region through various processing steps: before and after reduction and after reoxidation of the film. The initial bare Ru surface (marked "as installed") reveals two features. We attribute the peak located at ~531.6 eV to physisorbed species (e.g., carbon monoxide[41]), and the peak at ~530.2 eV to chemisorbed oxygen and hydroxyl radicals attached directly to Ru.[42] The presence of oxidic form of Ru is also confirmed by Ru $3d$ region (Fig. 4), where appropriate fitting requires inclusion of two spin-splitted pairs: metallic pair with Ru $3d_{5/2}$ peak located at 280.0 eV and oxidic one shifted by 0.7 eV toward higher binding energies (Ru $3d_{5/2}$ at 280.7 eV).[43] Ru $3d_{3/2}$ photoemission overlaps with C $1s$ lines from adventitious carbon and CO, which are present on the surface of as installed sample. However, C $1s$ contribution (not shown in Fig. 4) is very weak due to the low concentration of carbon and due to its much lower elemental sensitivity as compared to one of Ru.

Exposure of the surface to atomic H reduces Ru: both Ru–O component in Ru $3d$ region (Fig. 4; curve "Sn+H") and corresponding O $1s$ signal (Fig. 3) disappear. Still, some small amount of physisorbed species is detected in O $1s$ region as a result of readsorption of background gases during sample transfer between analysis and preparation chambers.

To mimic high pressure oxidation of the Sn-covered Ru film, we moved sample to preparation chamber and vented it. Air exposure resulted in reappearance of low energy peak in O $1s$ region (Fig. 3; curve "air"). Note that this oxide peak was shifted toward lower energy ~529.8 eV. The air exposure also led to 1.8 eV shift of Sn $3d$ pair toward higher binding energies (Fig. 7; curve air) resulting in the appearance of Sn $3d_{5/2}$ peak at 486.3 eV. These transformations in O $1s$ and Sn $3d$ regions are consistent with formation of SnO (Refs. 18 and 44) rather than SnO_2.[18,36] For SnO_2, it is expected a higher energy shift (2.2–2.5 eV) as well as appearance of O $1s$ oxide feature at binding energies higher than the one we observe in our spectra. The reaction affected nearly every Sn atom on the surface. Surprisingly, the air exposure of Ru film with Sn overlayer did not lead to oxidation of Ru. This is indicated by the absence of Ru–O components in O $1s$ (Fig. 3; curve air) and Ru $3d$ (Fig. 4; curve air) regions. After surface oxidation, the intensity of Ru $3d$ peak dropped down as seen from comparison of the signals measured from the same sample before [last data point in Fig. 2(a)] and after air exposure [first data point in Fig. 2(b)]. This is in contrast to the bare Ru film, where both Ru $3d$ and O $1s$ regions (not shown here) indicate that the surface reduced with ·H reoxidizes readily when exposed to the air.

G. Stability of Sn on Ru

We made an effort to remove Sn from Ru surface by flowing atomic H in the absence of Sn source. The dynamics of the regional signals is shown in Fig. 2(b) as a function of H dose. The figure demonstrates dramatic initial effect: an abrupt increase in Sn $3d$ and drop of O $1s$ signals due to reduction in the oxidized layer formed as a result of sample exposure to the air gases (to demount Sn source). Sn was rapidly reduced to metallic form by a relatively low dose of

·H as seen from backward chemical shift −1.8 eV of Sn 3*d* doublet (Fig. 7; compare curves air and "H only, 50 L") and from disappearance of oxidic component in O 1*s* region (Fig. 3).

Despite our expectation the prolonged ·H exposure did not lead to a substantial decrease in the Sn concentration on the surface (Fig. 7). After a H exposure of 1.9×10^{20} cm^{-2}, the surface still contained more than 90% of the initial Sn concentration. The stability of low coverages of Sn on Ru film with respect to ·H was recently noted by Fujima *et al.*,[27] who reported that blowing hydrogen radicals onto the surface removed Sn almost completely leaving some residual islands of Sn.

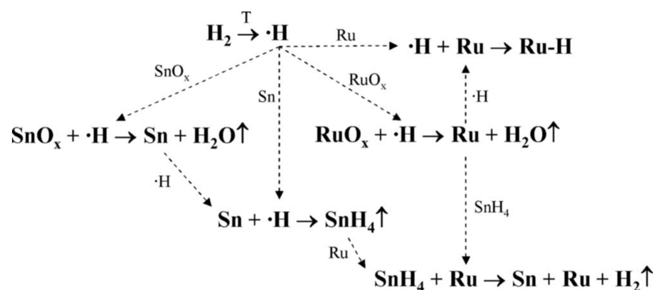

FIG. 8. Scheme of reaction pathways, which agrees with our experimental data. It indicates that atomic H, generated by cracking of H_2 on the hot filament, reduces RuO_x and SnO_x oxides, and reacts with Sn yielding SnH_4, which dissociatively adsorbs on Ru surface.

IV. DISCUSSION

A. Morphology of Ru film

Ruthenium layer used in our experiments was formed on Si substrate by magnetron sputtering technique. The properties of sputter produced films depend strongly on deposition conditions. Sputtered Ru films deposited by incident flux normal to the substrate are usually continuous and typically exhibit a normal texture.[45] The cross-sectional high-resolution transmission electron microscopy images[46] for 20 nm Ru film indicate a smooth layer with a columnar microstructure oriented vertically with respect to the substrate. At low deposition temperatures, Ru films are made of randomly oriented small grains[47] with typical size ranging from a few to tens of nanometers.[48] The grain size increases with deposition temperature and the texture with predominant ⟨0001⟩ orientation can be developed. At temperatures ≥400 °C, rf magnetron sputtering of Ru forms on Si substrate highly *c*-oriented films with smooth surface. We assume that our 31 nm thick Ru films are composed of {0001} domains with grain boundaries and amorphous patches occupying around 1% of the surface area.

B. Adsorption of ·H on Ru

Adsorption of molecular and atomic hydrogen on the (0001) and $(10\bar{1}0)$ planes of Ru has been studied extensively.[49–56] H_2 adsorbs on both planes dissociatively at all temperatures.[49,55,56] After dissociation the chemisorbed H on Ru(0001) is located exclusively at the fcc site[50] forming various structures as the coverage increases.

Low temperature (100 K) adsorption of atomic H on Ru(0001) surface was reported[52] to saturate at coverage 1.42 H adatoms per primitive surface unit cell. It is greater than a saturation coverage of 1 ML in the case of dissociative chemisorption of H_2. The threshold temperature of recombinative thermal desorption of hydrogen from this surface is ∼260–265 K with the desorption peak above RT, 320 K, accompanied by a wide shoulder at 380 K. The results are consistent with both fcc and hcp threefold hollow sites to be occupied at surface coverages above 1 ML. On the other plane of ruthenium, $Ru(10\bar{1}0)$,[51] adsorption of atomic H at 90 K also differs slightly from molecular hydrogen experiment producing additional thermal desorption peaks at 115 and 150 K. The authors reported that the coverage saturated at 2.5 ML. The highest temperature peak β_3 was at 340 K. The reported thermal desorption spectra[51] indicated that this state contains ∼30% of desorbing molecules.

The solubility of H in Ru at RT is very low.[57] Yates and co-workers[58,59] reported an evidence for the existence of a binding site for H below the first atomic layer of Ru atoms on the Ru(0001). The existence of subsurface H on Ru(0001) was reanalyzed and doubted in later studies.[50,60]

We expect that RT exposure of Ru polycrystalline film to a high flux of atomic H results in a high coverage of H adatoms (≤1 ML) (reaction $\cdot H + Ru \rightarrow Ru-H$ in Fig. 8). Neither of the techniques used in the present study can detect hydrogen on the surface. However, the evolution of LEIS measured under low current condition (Fig. 5) implicitly supports the idea that the surface of polycrystalline Ru film at RT is highly occupied when exposed to atomic H.

C. Reaction of ·H with Sn

In our experiments, both Ru and Sn are exposed to the mixture of atomic and molecular hydrogen. Sn is very reluctant in reaction with H_2; at RT it does not absorb any H_2.[61] There is an indication of some dissolution of H_2 at hydrogen pressures above 10 Torr.[62] In contrast, atomic H reacts readily with Sn to form tin hydride SnH_4,[63] which is volatile at RT (boiling point 221 K). Two binary hydrides of Sn known to date are stannane SnH_4 and distannane Sn_2H_6; both are characterized by covalent chemical bonding. The chemical ways of production of SnH_4 yield a small amount of Sn_2H_6 (Refs. 63–65) [can also be formed by vacuum ultraviolet decomposition of SnH_4 (Ref. 64)]. At RT, SnH_4 slowly decomposes to Sn and H.[65] This process is much faster at 370 K. Sn_2H_6 is extremely unstable above 160 K;[66] its half-life at RT is 4 s.[67] We believe that under our experimental conditions, atomic H impinging the surface of Sn droplet reacts with Sn producing SnH_4 (reaction $Sn + \cdot H \rightarrow SnH_4\uparrow$ in Fig. 8) and, possibly, some Sn_2H_6. The hydride desorbs into a gaseous form and reaches the surface of Ru.

D. Formation of Sn islands

We assume that SnH_4, which has a relatively low stability, readily dissociates at RT on the catalytically active surface of

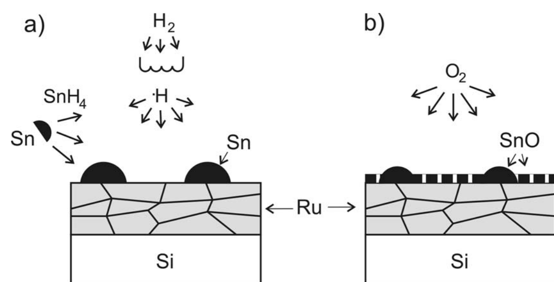

FIG. 9. Sketch illustrating the formation of Sn clusters on Ru film via SnH_4 dissociation (a) and spreading out of some cluster material after oxidation of Sn (b).

Ru (reaction $SnH_4 + Ru \rightarrow Sn + Ru + H_2\uparrow$ in Fig. 8). It is believed that *d*-band of transition metals plays an important role in dissociative adsorption.[68] The dissociation may proceed sequentially through several steps as it does in the case of silane (SiH_4) on Si(001) surface:[69]

$$SnH_4 \rightarrow \cdot SnH_3 \rightarrow \cdot SnH_2 \rightarrow \cdot SnH \rightarrow Sn.$$

This Sn transport mechanism illustrated by Fig. 9(a) is in agreement with our observation that a precursor, delivering Sn to Ru, originates from a diffuse source (Sec. III B). Nucleation of Sn may proceed via dehydrogenative coupling.[70] The role of surface defects in dissociation reactions is not clear but activation barrier for such process is probably very low.

Our microscopy data reveal nanometer scale islands of Sn with wide distribution of lateral dimensions (Fig. 6). The LEIS spectra show low occupation of the Ru surface (Fig. 5) indicating that there is no initial "buffer" layer wetting the surface. In combination these two observations are consistent with Volmer–Weber mechanism[71] of Sn growth on Ru film at RT. This is in contrast to the result reported for Ru(0001) at 330 K.[17] Thermal deposition of Sn led to Stranski–Krastanov growth mode, i.e., island growth over the initial two-dimensional (2D) layer. Another recent study[72] reports the results for vapor deposited Sn on thin Ru film protecting an optical structure. Their LEIS spectra are consistent with fractional surface occupation. We think that the surface of Ru polycrystalline film has a lower adhesive ability than the surface of a closed packed single crystal leading to the observed difference in Sn growth mechanisms.

The SEM image in Fig. 6 shows random distribution of Sn islands on Ru. We speculate that Sn nucleates at defect sites, presumably at grain boundaries, which usually exhibit a high interfacial energy and a weak bonding. It is not possible to deduce from our data whether SnH_4 adsorbs and dissociates on the grains to yield Sn diffusing to boundaries or it adsorbs at defect sites directly. Under our experimental conditions, Sn deposition is accompanied by adsorption of atomic H. We assume that a large surface area of Ru is occupied by H, which may hinder SnH_4 adsorption, and that the hydride has an easier access to the defect sites. Arena *et al.*[73] reported that the steps on Ru(0001) surface act as a repulsive barrier for H diffusion. The activation energy for diffusion along a terrace was measured 13.4 kJ/mol (0.14 eV), and for diffusion over a double atomic step 24.7 kJ/mol (0.26 eV). Within experimental error, they found no difference for diffusion up and down the step edges. In the recent theoretical study of dissociative adsorptions of SiH_4 and GeH_4 on a buckled SiGe(100)-2×1 surface, it was found that H preadsorption increased energy barrier for hydride adsorption.[74] Therefore, on Ru film with H overlayer, SnH_4 may mainly adsorb and dissociate at grain boundaries even if it is kinetically allowed for its fragments, produced on terraces, to diffuse to the selvedge region.

It is implicitly indicated by ion scattering spectra (Fig. 5) that ·H prefers to bind Ru and does not adsorb on Sn although one could expect an opposite preference just based on the Sn–H bond dissociation energy (264 ± 17 kJ/mol or 2.74 eV),[35,75] which exceeds the strength of Ru–H bond (223 ± 15 kJ/mol or 2.31 eV).[35] In the earlier study of atomic H adsorption on the $(\sqrt{3}\times\sqrt{3})$-$R30°$ Sn/Pt(111),[76] the hydrogen was also asserted to bind only to Pt atoms but not to Sn. In this case the Pt–H bond dissociation energy (330 kJ/mol or 3.42 eV) (Ref. 35) is higher than that of Sn–H as expected.

E. Oxidation of Sn/Ru film and reduction of surface oxides

The oxidations of neat Ru film and the film with Sn overlayer exhibit dramatic difference. Polycrystalline Ru surface oxidizes rapidly when exposed to the air. Natural oxidation affects presumably topmost Ru atoms and atoms at grain boundaries. Air exposure of Sn clusters on Ru film results in oxidation of nearly every Sn atom, but not Ru. The oxidation forms exclusively SnO with no higher oxides detected. There is a thermodynamic driving force for preferential oxidation of Sn as the heat of formation per oxygen atom of Sn oxide [SnO, 280.7 kJ/mol (Ref. 35) or 2.91 eV] is greater than that of Ru [RuO_2, 305 kJ/mol (Ref. 35) or 1.59 eV/O]. LEIS data indicate that before oxidation starts, the Sn atoms are aggregated in 3D islands, which occupy several percent of the surface. According to SEM images (Fig. 6), the air-exposed surface (i.e., the surface after high pressure oxidation) still contains Sn clusters although the area occupied on Ru surface is somewhat smaller. Also, XPS shows a drop of Ru signal [Fig. 2(b)] after oxidation. We speculate that the oxidation changes morphology of the film spreading a fraction of Sn islands across the Ru surface, as illustrated by Fig. 9(b). Photoelectrons emitted by Ru atoms are attenuated by thin Sn overlayer. Similar transformation was reported in earlier study of Fe adsorption on $TiO_2(110)$.[77] Oxidation of Fe clusters at 300 K flattened the overlayer, causing it to spread and completely cover the substrate at 1ML.

The effectiveness of atomic H in reducing oxides on thin Ru film ($\sim$2 nm) was studied earlier.[21] Atomic H could reduce the amount of oxide formed by irradiation of the surface Ru with $\sim$100 eV photons in the presence of H_2O. However, the extent of reduction was not clear due to the use of *ex situ* surface probe techniques, which led to reoxidation of the sample transported through the air. Another study[33] reports that at 300 K ·H removes chemisorbed O from the

single crystal Ru$(10\bar{1}0)$ nearly completely. However, thermally oxidized Ru with RuO_2 stoichiometry was more resistant to hydrogen, resulting in reduction in the top layer of RuO_2 at 300 K, while the bulk remained oxidized. Our photoelectron spectra measured in O 1*s* (Fig. 3) and Ru 3*d* (Fig. 4) regions show that ·H effectively removes the natural oxides from polycrystalline Ru film. Reaction proceeds via production of water,[51] which desorbs from the surface at RT (Fig. 8):

$$RuO_2 + 4H \rightarrow \ldots \rightarrow Ru + 2H_2O\uparrow .$$

Atomic H was also shown to reduce tin oxide: a thin film of tetragonal SnO supported on nickel gauze disappeared completely under the action of ·H.[78] In the recent study of influence of atomic H on transparent conducting oxides,[79] the authors observed a decrease in the transmittance of SnO_2 and detected the appearance of metallic Sn or SnO on the surface. In the present work, we observe that ·H is able to reduce both the tin oxide at Ru surface $[\mathrm{Sn(II)} \rightarrow \mathrm{Sn(0)}]$ and the bulk oxide $[\mathrm{Sn(IV)} \rightarrow \mathrm{Sn(0)}]$; some small amount of Sn(II) inside Sn source was probably unreachable by ·H.

V. CONCLUSION

The summary of our findings is illustrated by reaction pathway scheme in Fig. 8. Exposure of Sn to atomic H leads to gas-solid reaction, yielding stannane, SnH_4. At room temperature the hydride is a volatile gas with reduced stability. It is a precursor of Sn growth on Ru. SnH_4 adsorbs on the surface of polycrystalline Ru film [Fig. 9(a)] dissociatively. The thickest film grown in our study has an effective Sn coverage ~1 ML. It consists of randomly distributed 3D islands with an average size up to ~40 nm. Ion scattering data do not reveal the presence of initial 2D wetting layer. Therefore, we infer Volmer–Weber growth mode.[71] Nucleation of Sn occurs presumably at grain boundaries. This may result from combination of several factors as, for instance, a high interfacial energy at defect sites and a high coverage of H adatoms on Ru surface, hindering SnH_4 adsorption on terraces.

The high pressure oxidation of Sn islands on Ru at room temperature results in morphological transformation of the film spreading Sn across the Ru surface [Fig. 9(b)]. The oxidation forms exclusively SnO with no higher oxides detected, indicating a low dimensionality of oxidized Sn overlayer. No metallic Sn is found on this surface. The absence of any ruthenium oxide state indicates a strong charge transfer from Sn to Ru. This is in agreement with assumed morphological transformation of the film. Atomic H contends effectively against chemisorbed oxygen and natural oxides, which are present on Ru and Sn. It reduces RuO_2 to metallic Ru on bare Ru film, and SnO to metallic Sn on Sn/Ru film.

ACKNOWLEDGMENTS

The authors are grateful to Professor T. E. Madey (Physics Department, Rutgers University, Piscataway, NJ) and Professor P. C. Zalm (MiPlaza, Philips Research Europe, The Netherlands) for the helpful discussions, and to Dr. Sergij Yulin (Fraunhofer Institut Angewandte Optik und Feinmechanik, Jena, Germany) for the ruthenium thin film samples prepared for our experiments.

[1] J. G. Chen, C. A. Menning, and M. B. Zellner, Surf. Sci. Rep. **63**, 201 (2008).
[2] C. T. Campbell, Annu. Rev. Phys. Chem. **41**, 775 (1990).
[3] R. A. Buyanov and N. A. Pakhomov, Kinet. Catal. **42**, 64 (2001).
[4] P. Klusoň and L. Červený, Chem. Listy **91**, 100 (1997).
[5] T.-S. Tang, K.-Y. Cheah, F. Mizukami, S.-i. Niwa, and M. Toba, J. Am. Oil Chem. Soc. **71**, 501 (1994).
[6] S. M. dos Santos, A. M. Silva, E. Jordro, and M. A. Fraga, Catal. Today **107–108**, 250 (2005).
[7] A. C. B. Silva, A. P. G. de Sousa, J. D. Ardisson, H. G. L. Siebald, E. Moura, E. N. dos Santos, N. D. S. Mohallem, and R. M. Lago, Mater. Res. **6**, 137 (2003).
[8] J. Rodriguez and D. Wayne Goodman, Surf. Sci. Rep. **14**, 1 (1991).
[9] T. E. Madey, K. Pelhos, Q. Wu, R. Barnes, I. Ermanoski, W. Chen, J. J. Kolodziej, and J. E. Rowe, Proc. Natl. Acad. Sci. U.S.A. **99**, 6503 (2002).
[10] K. Mae and T. Honda, Thin Solid Films **373**, 199 (2000).
[11] M. R. Voss, H. Busse, and B. E. Koel, Surf. Sci. **414**, 330 (1998).
[12] Y. Li, M. R. Voss, N. Swami, Y.-L. Tsai, and B. E. Koel, Phys. Rev. B **56**, 15982 (1997).
[13] T. B. Massalski, J. L. Murray, L. H. Bennett, and H. Baker, *Binary Alloy Phase Diagrams* (American Society for Metals, Materials Park, OH, 1986).
[14] L. Perring, P. Feschotte, F. Bussy, and J. C. Gachon, J. Alloys Compd. **245**, 157 (1996).
[15] J. Charles, L. Perring, J. J. Kuntz, and J. C. Gachon, J. Phase Equilib. **20**, 573 (1999).
[16] S. Overbury, P. Bertrand, and G. Somorjai, Chem. Rev. (Washington, D.C.) **75**, 547 (1975).
[17] M. T. Paffett, A. D. Logan, and T. N. Taylor, J. Phys. Chem. **97**, 690 (1993).
[18] A. F. Lee and R. M. Lambert, Phys. Rev. B **58**, 4156 (1998).
[19] J. Wang, Y. Wang, S. Xie, M. Qiao, H. Li, and K. Fan, Appl. Catal., A **272**, 29 (2004).
[20] P.-Q. Yuan, Y.-M. Ma, Z.-M. Cheng, Y.-A. Zhu, and W.-K. Yuan, THEOCHEM **807**, 185 (2007).
[21] H. Oizumi, A. Izumi, K. Motai, I. Nishiyama, and A. Namiki, Jpn. J. Appl. Phys., Part 2 **46**, L633 (2007).
[22] S. A. Cotton, *Chemistry of Precious Metals* (Springer, New York, 1997).
[23] R. A. Meyers, *Encyclopedia of Physical Science and Technology* (Elsevier Science, New York, 2004).
[24] G. W. Schaeffer and S. M. Emelius, J. Am. Chem. Soc. **76**, 1203 (1954).
[25] H. O. Funsten, J. W. Boring, R. E. Johnson, and W. L. Brown, J. Appl. Phys. **71**, 1475 (1992).
[26] K. Börlin, T. Heinis, and M. Jungen, Chem. Phys. **103**, 93 (1986).
[27] K. Fujima, K. Hiraoka, I. Banno, Y. Yuba, and K. Nishihara, presented at the SPIE: Emerging Lithographic Technologies XII, San Jose, CA, 2008 (unpublished), Vol. 6921, p. 6921/6122.
[28] J. P. Allain, M. Nieto, M. Hendricks, A. Hassanein, C. Tarrio, S. Grantham, and V. Bakshi, presented at the Proceedings of SPIE: Emerging Lithographic Technologies XI, San Jose, CA, 2007, Vol. 6517, p. 65171V/65110.
[29] N. Fairley, CasaXPS 2.3.14 (Casa Software, Ltd.).
[30] J. John T. Yates, *Experimental Innovations in Surface Science: A Guide to Practical Laboratory Methods and Instruments* (Springer, New York, 1998).
[31] J. D. Wnuk, J. M. Gorham, B. A. Smith, M. Shin, and D. H. Fairbrother, J. Vac. Sci. Technol. A **25**, 621 (2007).
[32] V. Kagadei, E. Nefyodtsev, D. Proskurovsky, and S. Romanenko, Tech. Phys. Lett. **29**, 897 (2003).
[33] R. Wasielewski, B. V. Yakshinskiy, M. N. Hedhili, A. Ciszewski, and T. E. Madey, presented at the Proceedings of SPIE: 23rd European Mask and Lithography Conference, Grenoble, France, 2007, Vol. 6533, p. 653316.
[34] A. Salomonsson *et al.*, J. Nanopart. Res. **8**, 899 (2006).
[35] D. R. Lide, *CRC Handbook of Chemistry and Physics*, 88th ed. (CRC, Boca Raton, FL, 2007).

[36]M. A. Stranick and A. Moskwa, Surf. Sci. Spectra **2**, 50 (1993).
[37]H. H. Brongersma, M. Draxler, M. de Ridder, and P. Bauer, Surf. Sci. Rep. **62**, 63 (2007).
[38]Y. Wu, H.-S. Tao, E. Garfunkel, T. E. Madey, and N. D. Shinn, Surf. Sci. **336**, 123 (1995).
[39]J. P. Allain, A. Hassanein, M. Nieto, V. Titov, P. Plotkin, E. Hinson, B. J. Rice, R. Bristol, D. Rokusek, W. Lytle, B. J. Heuser, M. M. C. Allain, H. Ju, and C. Chrobak, presented at the Proceedings of SPIE: Emerging Lithographic Technologies IX, San Jose, CA, 2005, Vol. 5751, pp. 1110–1117.
[40]H. Seiler, J. Appl. Phys. **54**, R1 (1983).
[41]G. Rotaris, A. Baraldi, G. Comelli, M. Kiskinova, and R. Rosei, Surf. Sci. **359**, 1 (1996).
[42]N. S. Faradzhev, K. L. Kostov, P. Feulner, T. E. Madey, and D. Menzel, Chem. Phys. Lett. **415**, 165 (2005).
[43]Y. Kaga, Y. Abe, H. Yanagisawa, M. Kawamura, and K. Sasaki, Surf. Sci. Spectra **6**, 68 (1999).
[44]M. A. Stranick and A. Moskwa, Surf. Sci. Spectra **2**, 45 (1993).
[45]P. Morrow, F. Tang, T. Karabacak, P.-I. Wang, D.-X. Ye, G.-C. Wang, and T.-M. Lu, J. Vac. Sci. Technol. A **24**, 235 (2006).
[46]R. Chan, T. N. Arunagiri, Y. Zhang, O. Chyan, R. M. Wallace, M. J. Kim, and T. Q. Hurdc, Electrochem. Solid-State Lett. **7**, G154 (2004).
[47]H.-Y. Lee, Y.-W. Hsieh, C.-H. Hsu, and K. S. Liang, Mater. Chem. Phys. **82**, 984 (2003).
[48]R. Messier, A. P. Giri, and R. A. Roy, J. Vac. Sci. Technol. A **2**, 500 (1984).
[49]M. Tatarkhanov, F. Rose, E. Fomin, D. F. Ogletree, and M. Salmeron, Surf. Sci. **602**, 487 (2008).
[50]K. L. Kostov, W. Widdra, and D. Menzel, Surf. Sci. **560**, 130 (2004).
[51]E. Vesselli, G. Comelli, and R. Rosei, J. Chem. Phys. **120**, 8216 (2004).
[52]T. A. Jachimowski, B. Meng, D. F. Johnson, and W. H. Weinberg, J. Vac. Sci. Technol. A **13**, 1564 (1995).
[53]H. Busse, M. R. Voss, D. Jerdev, B. E. Koel, and M. T. Paffett, Surf. Sci. **490**, 133 (2001).
[54]M. J. Weiss, C. J. Hagedorn, and W. H. Weinberg, Surf. Sci. **429**, 54 (1999).
[55]R. Döll *et al.*, J. Chem. Phys. **108**, 8671 (1998).
[56]M. A. Barteau, J. Q. Broughton, and D. Menzel, Surf. Sci. **133**, 443 (1983).
[57]R. B. McLellan and W. A. Oates, Acta Metall. **21**, 181 (1973).
[58]J. T. Yates, Jr., C. H. F. Peden, J. E. Houston, and D. W. Goodman, Surf. Sci. **160**, 37 (1985).
[59]C. H. F. Peden, D. W. Goodman, J. E. Houston, and J. T. Yates, Jr., Surf. Sci. **194**, 92 (1988).
[60]P. Feulner, H. Pfnьr, P. Hofmann, and D. Menzel, Surf. Sci. **173**, L576 (1986).
[61]A. Sieverts, Zeit. Elektochem. **16**, 707 (1910).
[62]E. Baur and R. Brunner, Helv. Chim. Acta **17**, 958 (1934).
[63]T. G. Pearson, P. L. Robinson, and E. M. Stoddart, Proc. R. Soc. London, Ser. A **142**, 275 (1933).
[64]D. J. Aaserud and F. W. Lampe, J. Phys. Chem. **100**, 10215 (1996).
[65]N. N. Greenwood and A. Earnshaw, *Chemistry of the Elements*, 2nd ed. (Butterworth-Heinemann, Oxford, 1997).
[66]W. L. Jolly, J. Am. Chem. Soc. **83**, 335 (1961).
[67]D. J. Aaserud and F. W. Lampe, J. Phys. Chem. A **101**, 4114 (1997).
[68]R. I. Masel, *Principles of Adsorption and Reaction on Solid Surfaces* (Wiley, New York/IEEE, New York, 1996).
[69]T. Singh, M. S. Valipa, T. J. Mountziaris, and D. Maroudas, J. Chem. Phys. **127**, 194703 (2007).
[70]A. G. Davies, *Organotin Chemistry* (VCH, Weinheim, 1997).
[71]M. Volmer and A. Weber, Z. Phys. Chem. **119**, 277 (1926).
[72]J. P. Allain, M. Nieto, M. Hendricks, S. S. Harilal, and A. Hassanein, presented at the Proceedings of SPIE: Damage to VUV, EUV, and X-ray Optics, Prague, Czech Republic, 2007, Vol. 6586, p. 3.
[73]M. V. Arena, E. D. Westre, D. E. Brown, J. Kutzner, and S. M. George, Surf. Sci. **325**, 151 (1995).
[74]C.-L. Cheng, D.-S. Tsai, and J.-C. Jiang, Surf. Sci. **600**, 3194 (2006).
[75]L. May and C. R. Dillard, J. Chem. Phys. **34**, 694 (1961).
[76]E. Janin, M. Bjorkqvist, T. M. Grehk, M. Gothelid, C. M. Pradier, U. O. Karlsson, and A. Rosengren, Appl. Surf. Sci. **99**, 371 (1996).
[77]J.-M. Pan and T. E. Madey, J. Vac. Sci. Technol. A **11**, 1667 (1993).
[78]M. Piggott, Acta Crystallogr. **10**, 364 (1957).
[79]A. Masuda, K. Imamori, and H. Matsumura, Thin Solid Films **411**, 166 (2002).